Orbital Configuration of the Valence Electrons, Ligand Field Symmetry, and Manganese Oxidation States of the Photosynthetic Water Oxidizing Complex: Analysis of the S_2 State Multiline EPR Signals†

Ming Zheng and G. Charles Dismukes*

Hoyt Laboratory, Department of Chemistry, Princeton University, Princeton, New Jersey 08544

Received September 25, 1995⊗

A theoretical framework is presented for analysis of all three "multiline" EPR spectra (MLS) arising from the tetramanganese (Mn_4) cluster in the S_2 oxidation state of the photosynthetic water oxidizing complex (WOC). Accurate simulations are presented which include anisotropy of the *g* and (four) ^{55}Mn hyperfine tensors, chosen according to a database of ^{55}Mn(III) and ^{55}Mn(IV) hyperfine tensors obtained previously using unbiased least-squares spectral fitting routines. In view of the large (30%) anisotropy common to Mn(III) hyperfine tensors in all complexes, previous MLS simulations which have assumed isotropic hyperfine constants have required physically unrealistic parameters. A simple model is found which offers good simulations of both the native "19−21-line" MLS and the "26-line" NH_3-bound form of the MLS. Both a dimer-of-dimers and distorted-trigonal magnetic models are examined to describe the symmetry of the Heisenberg exchange interactions within the Mn_4 cluster and thus define the initial electronic basis states of the cluster. The effect of rhombic symmetry distortions is explicitly considered. Both magnetic models correspond to one of several possible structural models for the Mn_4 cluster proposed independently from Mn EXAFS studies. Simulated MLS were constructed for each of the eight (or seven) doublet states of the Mn_4 cluster in the WOC for the two viable oxidation models (3Mn(III)−1Mn(IV) or 3Mn(IV)−1Mn(III)), and using a wide range of axial Mn hyperfine tensors, with either coaxial or orthogonal tensor alignments. We find accurate simulations using the 3Mn(III)−1Mn(IV) oxidation model. In the dimer-of-dimers coupling model, the spin state conversion between two doublet states $|S_{12},S_{34},S_T|^7/_2,4,^1/_2\rangle$ and $|^7/_2,3,^1/_2\rangle$ is found to explain the large (25%) contraction in the hyperfine splitting observed upon conversion from the native MLS to the NH_3-bound MLS. Stabilization of this excited state as the new ground state is caused by change in the intermanganese exchange coupling, without appreciable change in the intrinsic hyperfine tensors. The lack of good simulations of the Ca^{2+}-depleted MLS suggests that Ca^{2+}-depletion changes both Mn ligation and intermanganese exchange coupling. The 3Mn(IV)−1Mn(III) oxidation model is disfavored because only approximate simulations could be found for the native MLS and no agreement with the NH_3-bound MLS was obtained. The scalar part of the hyperfine tensors for both Mn(III) and Mn(IV) ions were found to approximate (±5%) the values for the dimanganese(III,IV) catalase enzyme, suggesting similar overall ligand types. However, the large (30%) anisotropic part of the Mn(III) hyperfine interaction is opposite in sign to that found in all tetragonally extended six-coordinate Mn(III) ions (*i.e.*, the usual Jahn−Teller splitting). The distribution of spin density from the high-spin d^4 electron configuration of each Mn(III) ion corresponds to a flattened (oblate) ellipsoid. This electronic distribution is favored in five-coordinate ligand fields having trigonally compressed bipyramidal geometry, but it could also arise, in principle, in strained six-coordinate ligand fields having tetragonally compressed geometry, i.e. $[Mn_2(\mu\text{-O})]^{4+}$ (reverse Jahn−Teller distortion). The resulting valence electronic configurations are described as $e'^2e''^2$ and $(d_\pi)^3(d_{x^2-y^2})^1$, respectively, in contrast to the $(d_\pi)^3(d_{z^2})^1$ configuration common to unstrained six-coordinate tetragonally-extended Mn(III) ions, such as found in the $[Mn_2(\mu\text{-O})_2]^{3+}$ core in several synthetic dimers and catalase. Both of the former geometries predict strongly oxidizing Mn(III) ions, thereby suggesting a structural basis for the oxidative reactivity of the Mn_4 cluster in the WOC. The magnetic model needed to explain the MLS is not readily reconciled with the simplest structural and electronic models deduced from EXAFS studies of the WOC.

Introduction

Photosynthetic water oxidation, eq 1, is responsible for oxygen evolution in all green plants and algae. It is catalyzed

$$2H_2O \rightarrow O_2 + 4e^- + 4H^+ \qquad (1)$$

by the water oxidizing complex (WOC), an enzyme comprised of a tetramanganese cluster (Mn_4) bound at the interface between the Photosystem II reaction center protein complex and a "manganese stabilizing protein". Additionally, one Ca^{2+} ion and an undetermined number of Cl^- ions are essential inorganic cofactors which interact with the Mn_4 cluster in a structurally uncharacterized way.[1−3] Of the five metastable oxidation states of the WOC, S_0, ..., S_4, so-called "S states" in the terminology of Kok, O_2 is evolved only in the $S_4 \rightarrow S_0$ transition after sequential removal of four electrons and four protons. Presently, there is limited insight into the structure of the enzyme, and virtually nothing is known about the chemistry of how water is actually oxidized. Moreover, all of the many Mn_x cluster complexes which have been synthesized as models to date lack

† Dedicated to the memory of Professor Nobumasa Kitajima.

⊗ Abstract published in *Advance ACS Abstracts,* May 1, 1996.

(1) Debus, R. J. *Biochim. Biophys. Acta* **1992**, *1102*, 269−352.
(2) Dismukes, G. C.; Zheng, M.; Hutchins, R.; Philo, J. S. *Biochem. Soc. Trans.* **1994**, *22*, 323−327.
(3) Yachandra, V. K.; DeRose, V. J.; Latimer, M. J.; Mukerji, I.; Sauer, K.; Klein, M. P. *Science* **1993**, *260*, 675−679.

S0020-1669(95)01234-1 CCC: $12.00

functional activity as catalysts for water oxidation. This has stimulated the curiosity of enzymologists and chemists eager to understand the chemical basis for the unique reactivity of the enzyme.

The light-induced S_2 oxidation state of the WOC is the most extensively characterized S state. This state exhibits a "multiline" EPR signal (MLS) originating from ^{55}Mn hyperfine structure. The S_2 state is a mixed-valence paramagnetic $S = {}^1/_2$ ground state of the cluster.[4−6] This signal provided the first evidence indicating an electronically coupled binuclear or tetranuclear manganese cluster. Several forms of this signal are now known which depend upon treatments which disrupt the WOC.[7] The hyperfine "fingerprints" of the various S_2 state EPR signals are readily distinguished. The native MLS, which is produced in O_2-evolving samples by a single turnover of the dark-adapted S_1 state at 200 K or above, exhibits an average splitting of 82−88 G and 19−23 resolved lines depending on sensitivity for detection of the weak outer transitions. The overall spectral width of the native MLS is *ca*. 1900 G, arising almost entirely from the internal hyperfine field from ^{55}Mn. The similarity of the native MLS to the EPR signal formed by various dimanganese(III,IV) complexes in their ground doublet spin state (16-lines ca. 1250 G wide), suggested that the electronic ground state spin is also $S = {}^1/_2$ for the WOC.[4] In addition, on the basis of isotropic EPR spectral simulations, the 50% larger hyperfine field and additional lines in the MLS were considered as compelling evidence for a spin-coupled tetramanganese cluster composed of Mn(III) and Mn(IV) ions with spin $S = {}^1/_2$.[4,5,8,9] The possibility of a dimanganese(II,III) pair to account for the native S_2 state MLS was also considered[10] based largely on the prediction that this oxidation state should exhibit a 25% larger ^{55}Mn hyperfine field than dimanganese-(III,IV) dimers, as later demonstrated experimentally for mixed-valent dimers.[11] However, the dimanganese(II,III) proposal has been discarded based on the poor spectral agreement with simulations and the proposal's inability to account for the existence of more than one doublet spin state.[5,12−14] Accurate EPR simulations of the dimanganese(II,III) and -(III,IV) oxidation states of catalase which include both the g and hyperfine anisotropy further dispute the dimanganese(II,III) model for the WOC.[15] The possibility of a trimanganese model for the WOC was not precluded by the early analyses, other than the unlikelihood of achieving a ground doublet spin state for a trinuclear cluster. However, the trinuclear model has also been excluded based on poor agreement with isotropic spectral simulations.[12,14] The principal insight obtained to date from simulations of the native MLS, constrained by using isotropic hyperfine parameters, has been the Mn nuclearity (four) and Mn oxidation states, either 3Mn(III)−1Mn(IV) or 3Mn(IV)−1Mn(III).[8,12,14,16]

Due to the efforts of several groups there are now three distinct spectral forms of the S_2 MLS known, all centered at $g \sim 2$. A dark-stable "Ca^{2+}-depleted MLS" with asymmetric line shape is produced in samples which are inhibited by Ca^{2+} depletion using calcium chelators and illuminated above 250 K.[17−19] This MLS possesses more lines (at least 26) and an average ^{55}Mn hyperfine splitting which is 25% smaller than the native MLS, but with little change in the overall breadth of the ^{55}Mn hyperfine field. These changes indicate a major redistribution of spin density among the Mn ions, with only minor change in spin density transferred to the ligands.

A similar EPR spectral change occurs in the S_2 state upon binding ammonia at a Cl^- independent site.[20,21] This yields the "NH_3-bound MLS" which like the Ca^{2+}-depleted MLS has a 25% smaller hyperfine splitting (67.5 G), an increased number of hyperfine lines (∼26), but a more symmetrical line shape. The ^{14}N-hyperfine coupling to the Mn cluster, detected by ESEEM spectroscopy, provided strong evidence for direct coordination of ammonia to Mn.[22] Sr^{2+} substitution for Ca^{2+} in PSII also gives a MLS which is similar to the ammonia modified MLS, albeit with much weaker intensity.[23]

A third conformational state of the Mn cluster forms when the S_2 state is produced by illumination under conditions of either lower temperature (130 K instead of 200 K) or high concentrations of osmotic agents like sucrose.[24,25] Both treatments produce no MLS, but yield instead an unresolved resonance at $g = 4.1$ lacking hyperfine structure. Warming of the 130 K illuminated sample in the dark to ≥200 K converts this to the native MLS. The $g = 4.1$ signal can also be stabilized at higher temperatures by Cl^- depletion, F^- substitution, or addition of amines.[20,24,26,27] When formed by the latter treatment and using oriented PSII membranes, 16 or more ^{55}Mn hyperfine lines can be resolved. This further supports a tetrameric Mn_4 cluster as responsible for the EPR signal, and also that the hyperfine couplings must be anisotropic.[28] The $g = 4.1$ signal is currently considered to originate from stabilization of a ground electronic state with spin $S = {}^3/_2$ or ${}^5/_2$, suggesting that the intermanganese electron exchange interactions are sensitive to replacement of the endogenous inorganic cofactors, Cl^- and

(4) Dismukes, G. C.; Siderer, Y. *Proc. Natl. Acad. Sci. U.S.A.* **1981**, *78*, 274−278.
(5) Dismukes, G. C.; Ferris, K.; Watnick, P. *Photobiochem. Photobiophys.* **1982**, *3*, 243−256.
(6) Hansson, O.; Andreasson, L.-E. *Biochim. Biophys. Acta* **1982**, *679*, 261−268.
(7) Rutherford, A. W.; Boussac, A.; Zimmermann, J.-L. *New J. Chem.* **1991**, *15*, 491−500.
(8) Dismukes, G. C. In *Manganese in Metabolism and Enzyme Function*; Schram, V., Wedler, F. C., Eds.; Academic Press: New York, 1986; pp 275−309.
(9) dePaula, J. C.; Beck, W. F.; Brudvig, G. W. *J. Am. Chem. Soc.* **1986**, *108*, 4002−4009.
(10) Andreasson, L.-E.; Hansson, O.; Vanngard, T. *Chem. Scr.* **1983**, *21*, 71−74.
(11) Dismukes, G. C.; Sheats, J. E.; Smegal, J. A. *J. Am. Chem. Soc.* **1987**, *109*, 7202−7203.
(12) Dismukes, G. C. In *Mixed Valency Systems: Applications in Chemistry, Physics and Biology*; Prassides, K., Ed.; Kluwer Acad. Publ.: Dordrecht, The Netherlands, 1991; Vol. 343; pp 137−154.
(13) Andreasson, L.-E.; Vanngard, T. In *Encyclopedia of Inorganic Chemistry*; King, R. B., Ed.; John Wiley: New York, 1994.
(14) Bonvoisin, J.; Blondin, G.; Girerd, J. J.; Zimmermann, J. L. *Biophys. J.* **1992**, *61*, 1076−1086.
(15) Zheng, M.; Khangulov, S. V.; Dismukes, G. C.; Barynin, V. V. *Inorg. Chem.* **1994**, *33*, 382−387.
(16) Kusunoki, M. *Chem. Phys. Lett.* **1992**, *197*, 108−116.
(17) Boussac, A.; Zimmermann, J.-L.; Rutherford, A. W. *Biochemistry* **1989**, *28*, 8984−8989.
(18) Sivaraja, M.; Tso, J.; Dismukes, G. C. *Biochemistry* **1989**, *28*, 9459−9464.
(19) Ono, T.-A.; Inoue, Y. In *Current Research in Photosynthesis*; Baltischeffsky, M., Ed.; Kluwer Academic Press: Dordrecht, The Netherlands, 1990; Vol. I, pp 701-708.
(20) Beck, W. F.; de Paula, J. C.; Brudvig, G. W. *J. Am. Chem. Soc.* **1986**, *108*, 4018−4022.
(21) Andreasson, L.-E.; Hansson, O.; von Schenck, K. *Biochim. Biophys. Acta* **1988**, *936*, 351−360.
(22) Britt, R. D.; Zimmermann, J.-L.; Sauer, K.; Klein, M. P. *J. Am. Chem. Soc.* **1989**, *111*, 3522−3532.
(23) Boussac, A.; Rutherford, A. W. *Biochemistry* **1988**, *27*, 3476−3483.
(24) Casey, J. L.; Sauer, K. *Biochim. Biophys. Acta* **1984**, *767*, 21−28.
(25) Zimmermann, J.-L.; Rutherford, A. W. *Biochim. Biophys. Acta* **1984**, *767*, 7507−7511.
(26) Zimmermann, J.-L.; Rutherford, A. W. *Biochemistry* **1986**, *25*, 4609−4615.
(27) Ono, T.-A.; Nakayama, H.; Gleiter, H.; Inoue, Y.; Kawamori, A. *Arch. Biochem. Biophys.* **1987**, *256*, 618−624.
(28) Kim, D. H.; Britt, R. D.; Klein, M. P.; Sauer, K. *Biochemistry* **1992**, *31*, 541−547.
(29) Haddy, A.; Dunham, W. R.; Sands, R. H.; Aasa, R. *Biochim. Biophys. Acta* **1991**, *1099*, 25−34.

Ca^{2+}.[9,26,28,29] The structure of the Mn_4 cluster becomes more asymmetric and distorted in the S_2, $g = 4.1$ state, as revealed by Mn X-ray spectroscopy.[30]

The majority of previous EPR simulations of the MLS have been constrained by the assumption of isotropic hyperfine and **g** tensors. The assumption of isotropic ^{55}Mn hyperfine constants in these simulations was made because unconstrained simulations with five tensors (as many as 25 parameters) was a hopeless task. Unfortunately, this assumption is grossly unjustified, considering that Mn(III) typical exhibits quite large anisotropy ($A_{||} - A_{\perp} = 30\%$).[15,31,32] Inclusion of as little as 5% hyperfine anisotropy can eliminate any reasonable agreement between experimental and simulated spectra and thus models based solely on isotropic tensors are clearly misleading.[15] There are two major limitations to simulations using scalar hyperfine constants. First, this assumption leads to the prediction of incorrect oxidation states, since the hyperfine anisotropy of 30% is larger than the difference in scalar hyperfine constants for different oxidation states. Second, scalar hyperfine constants do not give any information concerning the spatial distribution of the Mn electron spins in the cluster. Since there are large differences in the symmetry of the spin density surrounding Mn(II), Mn(III), and Mn(IV) ions, the hyperfine anisotropy alone offers a more precise means to determine both the Mn oxidation state and, in particular, the orbital configuration of the unpaired electrons. The latter information has not been previously determined for the WOC and provides the bridge between the electronic structure and the ligand reactivity which is essential to elucidating the mechanism of water oxidation.

Reasonably good simulations of the native S_2 MLS have been reported for data obtained at X- and Q-band frequencies (9 and 34 GHz, respectively) and rather poor agreement with the S-band spectrum (3.4 GHz), by using a Mn(III)−Mn(IV) dimer model which allows unconstrained anisotropy of both the magnetic hyperfine and nuclear-electric quadrupole tensors for both Mn ions.[33] This study stresses the possible importance of both of these interactions. They ascribe the complexity of the normal MLS to extremely anisotropic parameters derived from an unprecedented ligand field splitting around both Mn ions. The model did not explain the other forms of the MLS. We shall address this model in detail in the Discussion.

Until now there has been no general theory which accounts for the multiple spectral forms of the MLS in a single model. Moreover, limited understanding exists of the nature of the structural changes which occur at the Mn_4 cluster as a result of the aforementioned treatments. Here we present a model to account for the multiple spectral forms of the MLS which eliminates the use of the unconstrained fitting parameters and is firmly based on the magnetic hyperfine parameters of Mn(III) and Mn(IV) sites in complexes and proteins.[15,34−36] Preliminary accounts of this work have been given.[2,37,38]

Methods

Analysis of the magnetic and EPR properties of spin-coupled clusters of paramagnetic ions is a well-developed experimental and theoretical subject from which the present analysis is derived.[39−41] Implementation of the existing theory needs to explain the following features of the WOC within a single model: (1) give an accurate simulation of the anisotropic line shape of the MLS; (2) account for the ^{55}Mn hyperfine changes upon interconversion between chemically modified forms of the WOC; (3) be compatible with the previous assignment of the $g = 4.1$ EPR spectral form of the WOC as an $S \geq {}^3/_2$ spin state of a Mn tetramer; (4) be compatible with the structural data from Mn EXAFS spectroscopy.[3]

We begin by first describing developments which have limited the reasonable choices for Mn(III) and Mn(IV) hyperfine tensor elements for the WOC.[15,38] This will be followed by a presentation of the dimer-of-dimers and the distorted-trigonal exchange coupling models for the Mn_4 cluster and how they are used to relate the Mn_4 cluster hyperfine parameters obtained from the simulations to the intrinsic (monomeric) hyperfine parameters and Mn oxidation states. The simulations will then follow, and we will end with our interpretation of the results and comparisons to previous work.

All multiline signals presented in this work are from spinach PSII membranes or core complexes and have the central 30 G wide region removed where overlap with tyrosine radicals occurs. However, essentially the same spectra are obtained in blue-green alga like the thermophilic *Synechococus elongatus* and the non-thermophile *Synechocystis sp* PCC6803. To our knowledge, the multiline signals and the Mn_4 cluster from which they arise are universal features of all oxygenic photosynthetic organisms, from the most primitive cyanobacteria to modern plants.

Analysis

Coordinated Ligands to the WOC(S_2) and Mn Catalase-(III,IV). There is compelling evidence from ENDOR, ESEEM, and X-ray spectroscopies which now indicates that the ligands to the Mn ions of the WOC are probably very similar to those which bind the Mn ions in Mn catalase(III,IV).[15,35−37,42,43] For the WOC the spectroscopic data have revealed 1−2 protein-derived nitrogen ligands per Mn_4 cluster[34−36] and that histidine is directly implicated.[35] Histidine ligation is also supported by chemical modification studies.[44−46] The remaining ligands are generally considered to include a pair of (μ-O)$_2$ bridges between two pairs of Mn ions, on the basis of the short Mn−Mn distance observed by EXAFS.[3] Also carboxylatos are candidates for Mn ligands on the basis that this group lacks magnetic nuclei in the first and second coordination shells and thus offers the simplest explanation of the lack of strong proton hyperfine couplings.[34]

Mn Oxidation States in the S_2 State. To interpret the MLS one needs to know the effective spin Hamiltonian for the EPR active ground state. It has been recognized for some time that the MLS must be attributable to a doublet spin state.[4,5] On this basis it has long been realized that there are only two possible Mn_4 oxidation states for the S_2 state, 3Mn(III)−1Mn(IV) or

(30) Liang, W.; Latimer, M. J.; Dau, H.; Roelofs, T. A.; Yachandra, V. K.; Sauser, K.; Klein, M. P. *Biochemistry* **1994**, *33*, 4923−4932.
(31) Gerritsen, H. J.; Sabisky, E. S. *Phys. Rev.* **1963**, *132*, 1507−1512.
(32) Vanngard, T.; Hansson, O.; Haddy, A. In *Manganese Redox Enzymes*; Pecoraro, V. L., Ed.; VCH: New York, 1992; pp 105−118.
(33) Ahrling, K. A.; Pace, R. J. *Biophys. J.* **1995**, *68*, 2081−2090.
(34) Tang, X.-S.; Sivaraja, M.; Dismukes, G. C. *J. Am. Chem. Soc.* **1993**, 2382−2389.
(35) Tang, X.-S.; Diner, B. A.; Larsen, B. S.; Gilchrist, M. L., Jr.; Lorigan, G. A.; Britt, R. D. *Proc. Natl. Acad. Sci. U.S.A.* **1994**, *91*, 704−708.
(36) DeRose, V. J.; Yachandra, V. K.; McDermott, A. E.; Britt, R. D.; Sauer, K.; Klein, M. P. *Biochemistry* **1991**, *30*, 1335−1341.
(37) Dismukes, G. C.; Tang, X.-S.; Khangulov, S. V.; Sivaraja, M.; Pessiki, P.; Zheng, M. *Research in Photosynthesis*; Kluwer Academic Publ.: Dordrecht, The Netherlands, 1992; Vol. II, pp 257−264.
(38) Zheng, M.; Dismukes, G. C. In *Research in Photosynthesis*; Murata, N., Ed.; Kluwer Academic Publ.: Dordrecht, The Netherlands, 1992; Vol. II, pp 305−308.
(39) Sinn, E. *Coord. Chem. Rev.* **1970**, *5*, 313−347.
(40) Tsukerblat, B. S.; Belinskii, M. I.; Fainzil'berg, V. E. *Sov. Sci. Rev.: B. Chem.* **1987**, *9*, 337−481.
(41) Belinskii, M. I. *Chem. Phys.* **1994**, *179*, 1−22.
(42) Khangulov, S. V.; Sivaraja, M.; V., B. V.; Dismukes, G. C. *Biochemistry* **1993**, *32*, 4912−4924.
(43) Waldo, G. S.; Yu, S.; Penner-Hahn, J. E. *J. Am. Chem. Soc.* **1992**, *114*, 5869−5870.
(44) Preston, C.; Seibert, M. In *Current Research in Photosynthesis*; Baltscheffsky, M., Ed.; Kluwer Academic Press: Dordrecht, The Netherlands, 1990; Vol. I, pp 925-928.
(45) Tamura, N.; Ikeuchi, M.; Inoue, Y. *Biochim. Biophys. Acta* **1989**, *973*, 281−289.
(46) Seibert, M.; Tamura, N.; Inoue, Y. *Biochim. Biophys. Acta* **1989**, *974*, 185−191.

Table 1

(a) Simulation Parameters used for the Mn Catalase(III,IV) EPR Spectrum[a]

A_x, A_y, A_z			
Mn(III)	Mn(IV)	g_x, g_y, g_z	R, %
−410, −425, −315	235, 224, 252	2.014, 2.014, 2.000	4.5

(b) Intrinsic ^{55}Mn Hyperfine Parameters for Mn(III) and Mn(IV) in Mn Catalase(III,IV)[b]

	Mn(III)	Mn(IV)
a_x, a_y, a_z	−218, −218, −158	−230, −230, −252
$\|a_{iso}\|$	192 (or 68.5 G)	237 (or 84.6 G)
$a_z - a_x$	55	−22
$(a_x, a_y, a_z)^c$	−174, −174, −228	−230, −230, −252

[a] A_x, A_y, and A_z: effective hyperfine tensor elements (MHz). R is a measure of the goodness of fit (see ref 15). [b] $|a_{iso}|$ and $a_z - a_x$ refer to the isotropic and anisotropic part, respectively, of the intrinsic mononuclear hyperfine tensor. [For the sake of simplicity, the slight rhombicity of the effective hyperfine tensors listed in part a is ignored and the average value of A_x and A_y was taken when converting them to the corresponding intrinsic hyperfine element.] Units: MHz. [c] Hyperfine tensor obtained when the sign of $a_z - a_x$ is reversed.

3Mn(IV)−1Mn(III).[5,12] These are the only two Mn_4 oxidation states we shall consider.

The Choice of Intrinsic Monomer Hyperfine Constants for ^{55}Mn. In Table 1 we list the isotropic and anisotropic hyperfine parameters for Mn(III) and Mn(IV) ions from *T. thermophilus* catalase. The scalar hyperfine interaction is a sensitive function of the ligand type and should not be assumed to be a free parameter for simulating the MLS, since the WOC is known to contain predominantly oxygen type lignads. We explored a wide range of hyperfine tensors with scalar magnitudes centered at the Mn catalase value and ranging over ±15%, which covers all possible N/O ratios simulated to date.

Another important aspect revealed by EPR studies of Mn catalase and Mn complexes is the very anisotropic nature of Mn(III) hyperfine tensors. The anisotropy arises from the dipolar interaction between the nuclear spin and the asymmetric high-spin d^4 orbital configuration. The hyperfine anisotropy for Mn(III) arising from the valence atomic orbital configuration in a tetragonally distorted octahedral environment (with $a_x = a_y$) has been evaluated,[31] eq 2, where the "+' and "-" signs

$$\Delta a = a_z - a_x = \pm {}^3/_{14} g_e \beta_e g_l \beta_l \langle r^{-3} \rangle \qquad (2)$$

apply to the $(d_\pi)^3(d_{z^2})^1$ and $(d_\pi)^3(d_{x^2-y^2})^1$ configurations, respectively. Since the electronic configuration of Mn ions in WOC is unknown, we allow the hyperfine anisotropy for Mn(III) to have either a + or a − sign.

We also found that colinear Mn hyperfine tensors gave the best MLS simulation. Several different orthogonal combinations for the relative orientations of the four hyperfine tensors were also examined to see if the resulting simulations could better describe the MLS. Although this was not found to be the case, the result is summarized in the **Simulations** section for completeness.

Effective Spin Hamiltonian for EPR Simulations. To evaluate the EPR and magnetic properties of an isolated doublet state of the cluster there are two factors to consider: the composition of the state in terms of how much of each ion's spin contributes, and the method for calculating the effective hyperfine constants from the intrinsic (monomeric) ones. The latter part is well established by application of angular momentum theory[47,48] and we shall only summarize the terminology needed here.[5,12]

We consider initially two terms in the Hamiltonian expression, eq 3, the Zeeman interaction of the total spin $\mathbf{S}_T$, defined as $\sum_i \mathbf{S}_i$, with the external magnetic field $\mathbf{H}$, and the hyperfine interaction of each Mn spin $\mathbf{S}_i$ with the nuclear spin of the same atom $\mathbf{I}_i$.

$$\boldsymbol{H} = g\beta \mathbf{S}_T \mathbf{H} + \sum_{i=1}^{4} \mathbf{S}_i \mathbf{a}_i \mathbf{I}_i \qquad (3a)$$

In this expression, the $\mathbf{a}_i$'s are the intrinsic (monomeric) hyperfine tensors. We shall evaluate properties within the $\mathbf{S}_T$ subspace owing to the expected dominance of the interion exchange interactions ($|J| \gg$ zero-field splittings) as observed in $Mn^{III}Mn^{IV}$ complexes; the matrix elements of $\mathbf{S}_i$ can then be evaluated via angular momentum theory. For the two exchange coupling schemes we are going to consider, Wigner−Eckart theorem has been used. The result is that each $\mathbf{S}_i$ can be replaced by the product of a constant times the total spin operator, $\mathbf{S}_i = p_i \mathbf{S}_T$. Here the constant p_i is the projection of the atomic electron spin onto the total spin, formally

$$p_i = \frac{\langle |\mathbf{S}_i \cdot \mathbf{S}_T| \rangle}{\mathbf{S}_T{}^2}$$

where the bracket notation, $|\ \rangle$, represents any of the states with $S_T = {}^1/_2$. With these replacements, eq 3a is transformed into a readily usable form, eq 3b, and our task is complete provided that we know the effective "tetramer" hyperfine tensors, $p_i \mathbf{a}_i$.

$$\boldsymbol{H} = g\beta \mathbf{S}_T \mathbf{H} + \sum_{i=1}^{4} \mathbf{S}_T (p_i \mathbf{a}_i) \mathbf{I}_i \qquad (3b)$$

This is the usual starting place for consideration of the magnetic properties of a strongly coupled cluster with an isolated ground state. From here, one can adopt different approaches to account for the magnetic properties. An obvious one is to treat each $p_i \mathbf{a}_i$ as a *single* parameter, obtainable through a spectral fitting procedure, and then seek a physical explanation for each parameter. The problem with this approach is that the fitting procedure is very tedious for four nuclei, since there could be as many as 15 principal values for the g plus four hyperfine tensors and 10 Euler angles representing their relative orientations. It is virtually impossible to obtain a unique solution with so many parameters. An unrestricted fitting procedure has been adopted by Bonvoisin et al.[14] and Kusunoki[16] with the necessary oversimplification that all parameters were assumed to be scalars.

Instead, we approach this problem by treating p_i and $\mathbf{a}_i$ separately and make full use of the knowledge of the intrinsic Mn hyperfine tensors and their orientations obtained from simulations of model complexes and proteins. Expressions for p_i can be derived which enable the intrinsic hyperfine tensors, $\mathbf{a}_i$, to be scaled to obtain the tetramer hyperfine tensors, provided an exchange coupling model is available.[5,12,48] Simulation of the EPR signals from the different spin states of a Mn tetramer can then be undertaken, and only the relative orientations of the tensor axes needs to be established. The orientations of the ^{55}Mn hyperfine and $\mathbf{g}$ tensor axes are unknown for the WOC, although anisotropy data from Mn EXAFS and EPR multiline studies in partially ordered membrane preparations do offer constraints which guide this choice. As noted above, we shall

(47) Tinkham, M. *Group Theory and Quantum Mechanics*; McGraw-Hill: New York, 1964.
(48) Bencini, C.; Gatteschi, D. *EPR of Exhange Coupled Systems*; Springer-Verlag: Berlin, 1990.

make use of the observation that for $(\mu\text{-O})_2$-bridged $Mn^{III}Mn^{IV}$ dimers the hyperfine and **g** tensors are essentially axial and strictly collinear.

Exchange Coupling Models. The Dimer-of-Dimers Model. The next step is to determine the spin composition of each of the EPR active doublet states with $S_T = {}^1/_2$ in terms of the individual contributions from each of the four Mn ions; *i.e.*, we need to know the spin wave functions. By definition the ground state is obtained by solving the complete Hamiltonian of the Mn cluster, $\boldsymbol{H} = \boldsymbol{H}(\sigma,\mathbf{S}_1,\mathbf{S}_2,\mathbf{S}_3,\mathbf{S}_4)$, where σ represents dependence on parameters other than spin. It is common practice to parametrize this Hamiltonian using an effective spin exchange Hamiltonian which can account for the energies and spin multiplicities of the electronic states. The most successful general form applicable to weakly coupled atoms is the Heisenberg−Dirac−Van Vleck exchange Hamiltonian, eq 4.

$$\boldsymbol{H}_{ex} = \sum_{i>k=1}^{4} 2j_{ik}\,\mathbf{S}_i\mathbf{S}_k \qquad (4)$$

The resulting spin functions can be used to calculate physical observable, like the EPR spectrum.[49] Equation 4 is insufficient to describe the electronic states of a cluster when anisotropic zero-field splitting (ZFS) are comparable to the j_{ik} values.[50] All $(\mu\text{-O})_2$ bridged $Mn^{III}Mn^{IV}$ dimers have large exchange interactions ($J \gg$ ZFS), resulting in a well-isolated doublet ground state having an EPR signal that is readily simulated without the need to include ZFS.[15] Accordingly, we may justifiably assume eq 4 offers a valid description of the doublet states of the WOC.

Even with this simplification, to solve for the ground state functions for the general case of no symmetry (all J's different) cannot be done analytically. For tetramers with high enough symmetry that there are only three unique J's, the Kambe procedure has been used to obtain the eigenfunctions and energies of the states.[39,51] The effects of this simplification can be relaxed later using more general methods for solving eq 4 which allow lower symmetries to be considered.[41] A promising exchange Hamiltonian which requires only three J's is eq 5a or its equivalent form eq 5b, the "dimer-of-dimers" magnetic Hamiltonian, for which the model is depicted in Chart 1A. Equation 5 is compatible with the EXAFS structural data, suggesting a possible "dimer-of-dimers" spatial arrangement of the four Mn ions in the WOC (one of nine possible arrangements).[3,52] In this model two pairs of $Mn_2(\mu\text{-O})_2$ units form intradimer separations of 2.7 Å that are linked on one edge by a longer Mn−Mn vector of 3.3 Å. In eq 5, $\mathbf{S}_{12} = \mathbf{S}_1 + \mathbf{S}_2$ and

$$\boldsymbol{H}_{ex} = -2J\mathbf{S}_{12}\mathbf{S}_{34} - 2J_{12}\mathbf{S}_1\mathbf{S}_2 - 2J_{34}\mathbf{S}_3\mathbf{S}_4 \qquad (5a)$$

$$\boldsymbol{H}_{ex} = -J\mathbf{S}_T{}^2 - J_{12}\mathbf{S}_{12}{}^2 - J_{34}\mathbf{S}_{34}{}^2 \qquad (5b)$$

$\mathbf{S}_{34} = \mathbf{S}_3 + \mathbf{S}_4$ are the intermediate dimer spin vectors. The dimer-of-dimers magnetic model has been shown to offer a proper description of the ground and low-lying excited spins states of a structurally characterized Mn tetramer comprised of two $Mn_2(\mu\text{-O})_2$ units bridged symmetrically by two alkoxide ligands.[53]

Chart 1

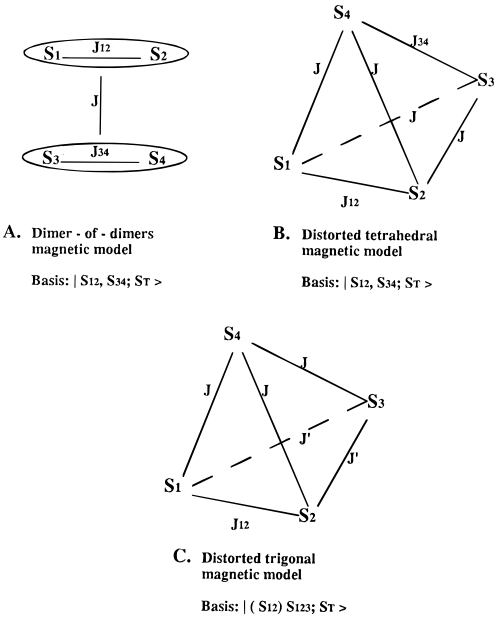

Equation 5a is isomorphic with a slightly more general Hamiltonian, eq 5c, corresponding to a distorted tetrahedron in which all four of the interdimer J's are equal, as depicted in Chart 1B. This distorted tetrahedral model was previously used to calculate the first simulations of the MLS using isotropic hyperfine constants.[5]

$$\boldsymbol{H}_{ex} = -2J_{12}\mathbf{S}_1\mathbf{S}_2 - 2J_{34}\mathbf{S}_3\mathbf{S}_4 - 2J(\mathbf{S}_1\mathbf{S}_3 + \mathbf{S}_1\mathbf{S}_4 + \mathbf{S}_2\mathbf{S}_3 + \mathbf{S}_2\mathbf{S}_4) \qquad (5c)$$

The energies resulting from solution of eq 5b are given by eq 6a, while those for eq 5c are given by eq 6b.[39]

$$E(S_{12},S_{34},S_T) = -JS_T(S_T+1) - J_{12}S_{12}(S_{12}+1) - J_{34}S_{34}(S_{34}+1) \qquad (6a)$$

$$E(S_{12},S_{34},S_T) = -JS_T(S_T+1) - (J_{12}-J)[S_{12}(S_{12}+1)] - (J_{34}-J)[S_{34}(S_{34}+1)] \qquad (6b)$$

As expected on the basis of the symmetry under permutation of indices, (12)(34), both of these cases depend on the same three spin vectors, have the same basis set ($|S_{12},S_{34},S_T\rangle$) and energy level scheme, and allow for any of the possible doublet states to become the ground state, depending on the values of J_{12}/J and J_{34}/J. Accordingly, we need only consider the simpler Hamiltonian, eq 5a, in the present analysis. For the case of a cluster with 3Mn(IV)−1Mn(III) or 3Mn(IV)−1Mn(III) there are eight and seven doublet states possible, respectively. These will be nondegenerate for all cases in which the permutational symmetry of the exchange Hamiltonian is lower than cubic (S_4). Since each doublet state is a potential candidate for the ground state, we wish to consider the range of exchange coupling parameters which enables each doublet state to become the ground state.

Figure 1 is a "spin state probability diagram" which plots all of the doublet spin functions that are predicted by eq 5a or eq 5c to be the lowest energy states for certain range of the reduced exchange parameters, $J_{12}/|J|$ and $J_{34}/|J|$, for the case of 3Mn(III)−1Mn(IV). A proof is given in the Supporting Information on how to construct this diagram. The area occupied by each spin function in this plot indicates the range of exchange parameters which lead to this doublet state being the lowest

(49) Griffith, J. S. *Mol. Phys.* **1972**, *24*, 833−842.
(50) Sage, J. T.; Xia, Y.-M.; Debrunner, P. G.; Keough, D. T.; de Jersey, J.; Zerner, B. *J. Am. Chem. Soc.* **1989**, *111*, 7239−7247.
(51) Kambe, K. *J. Phys. Soc. Jpn.* **1950**, *5*, 48−51.
(52) DeRose, V. J.; Mukerjee, I.; Latimer, M. J.; Yachandra, V. K.; Sauer, K.; Klein, M. P. *J. Am. Chem. Soc.* **1994**, *116*, 5239−5249.
(53) Kirk, M. L.; Chan, M. K.; Armstrong, W. H.; Solomon, E. I. *J. Am. Chem. Soc.* **1992**, *114*, 10432−10440.

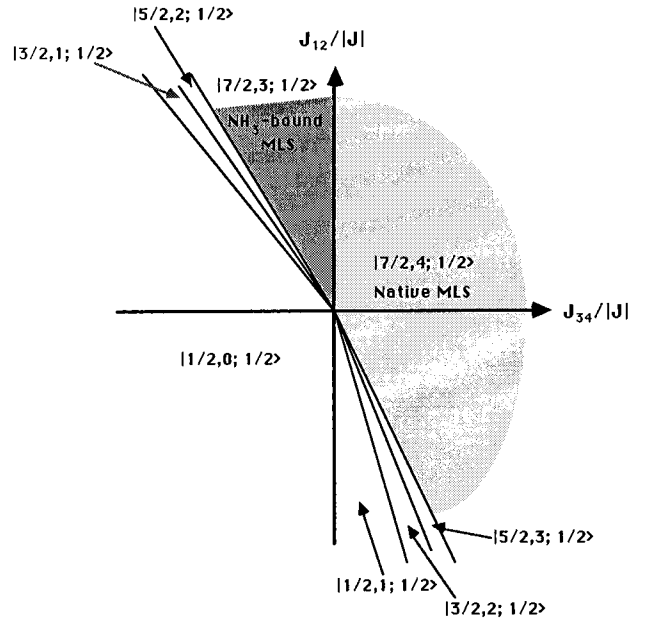

Figure 1. Spin phase diagram for the Mn cluster of the WOC. Oxidation model: 3Mn(III)−1Mn(IV). Exchange coupling scheme: dimer-of-dimers (eq 6). The area occupied by each spin state indicates the range of the reduced intradimer couplings $J_{12}/|J|$, $J_{34}/|J|$ (with $J < 0$) that lead to the indicated doublet states to be the ground state.

energy state. The area can be thought of as the probability that each of the doublet states would be the ground state, if any possible value of reduced exchange parameters could be realized. It is clear from this figure that the most probable doublet states which occur are $|^7/_2,4,^1/_2\rangle$ and $|^1/_2,0,^1/_2\rangle$ followed by $|^7/_2,3,^1/_2\rangle$ and $|^1/_2,1,^1/_2\rangle$. The five remaining spin states occupy very little area and hence would be unlikely to exist unless a very specific combination of J_{12} and J_{34} were to occur. This model suggests that if all intermanganes exchange interactions which produce doublet ground states were equally probable, then only these four basis states are likely to arise as major components of the true eigenstates, even under lower symmetry exchange models. Despite this simplifying condition, we *have examined all possible doublet states in the MLS simulations*. The eigenstates and their spin projections are summarized in Tables A2, A3, and A4 in the Supporting Information.

Distorted-Trigonal Coupling Model. A second tetramer coupling model was examined which exhibits C_s point symmetry which we term distorted-trigonal symmetry, as depicted in Chart 1C. In this model, $\mathbf{S}_1$ and $\mathbf{S}_2$ are coupled to give the intermediate spin $\mathbf{S}_{12}$, which is then coupled to the third spin $\mathbf{S}_3$ to give $\mathbf{S}_{123}$ intermediate spin. Finally $\mathbf{S}_{123}$ is coupled to $\mathbf{S}_4$ to give the total spin $\mathbf{S}_T$. The spin state vectors may be expressed as $|(S_{12})$-$S_{123},S_T\rangle$. The HDVV spin exchange Hamiltonian for this scheme can be expressed as eq 7a. The resulting energy expression is given by eq 7b. The corresponding expressions for the

$$H = -2J\mathbf{S}_4(\mathbf{S}_1 + \mathbf{S}_2 + \mathbf{S}_3) - 2J'\mathbf{S}_3(\mathbf{S}_1 + \mathbf{S}_2) - 2J_{12}\mathbf{S}_1\mathbf{S}_2 \quad (7a)$$

$$E(J_{12},J_{123},J) = -J[S_T(S_T + 1) - S_{123}(S_{123} + 1)] - J'[S_{123}(S_{123} + 1) - S_{12}(S_{12} + 1)] - J_{12}S_{12}(S_{12} + 1) \quad (7b)$$

eigenstates and the p_i projections are given in the Supporting Information. Refer to Tables A2, A3, and A4. This magnetic model also corresponds to one of the nine possible structural models which have been proposed as consistent with the available EXAFS data for the Mn_4 cluster (Figure 9E in ref 52). The trigonal coupling scheme has also been used recently to describe the magnetic properties of oxidized Fe_4S_4 high-potential iron−sulfur proteins,[54] which are believed to have trigonal structure (C_{3v}), as well as the trigonal distorted cubane cores $[Mn_4O_3Cl]^{6+}$.[55]

MLS EPR Simulation Method. Because the sum of the absolute values of the tetramer hyperfine tensors is directly proportional to the spectral breadth, we may impose the experimental constraint given by eq 8.[12,14,56] This constraint is

$$\sum_{i=1}^{4}|p_i\mathbf{a}_i| = {}^1/_5(\text{spectral breadth}) \quad (8)$$

obtained by solving eq 3b. It is an approximation that neglects contributions, estimated to be less than 5%, to the spectral breadth from higher order terms in $(A/2g\beta H)^n$ for $n \geq 2$. We can experimentally determine the limited range of p_i projections which could be responsible for producing the overall breadth of the MLS by choosing average intrinsic hyperfine tensors for Mn(III) and Mn(IV). Because the total spectral breadth of the MLS is about 1900 G, this requires that the sum of $|p_i|$'s is about 5, if one takes 80 G as an average intrinsic hyperfine constant for the four Mn ions. This criterion eliminates 27 out of 32 of the doublet spin states listed in Table A3 and 26 out of 28 states given in Table A4. Thus another reason for the appropriateness of the simplified exchange Hamiltonians, eqs 6 and 7, is that only a few states having large projections can possibly contribute to the MLS.

All spectral simulations were generated using a FORTRAN program which is a simple extension of an existing one we have been using for Mn dimer EPR simulations.[15,56] This program is capable of handling four $I = {}^5/_2$ hyperfine tensors plus the **g** tensor with axial symmetry, and determines powder line shapes by integration over a spherical quadrant. The eigenvalues of the effective spin Hamiltonian are obtained to second order in $A^2/g\beta H$, and the resonance field is then obtained by solving a second-order algebraic equation. An isotropic Lorentzian line shape of uniform width was used for all transitions. These conventional conditions apply to all EPR spectra and produce high quality simulations of both $Mn^{II}Mn^{III}$ and $Mn^{III}Mn^{IV}$ dimers with statistical R values below 4.5%.[15]

For each doublet spin state in each model we construct a set of effective (tetramer) hyperfine tensors defined as $A_i = p_i\mathbf{a}$(III) or $A_i = p_i\mathbf{a}$(IV) in which **a**(III) and **a**(IV) are the intrinsic hyperfine tensors of each ion. In addition, the **g** tensor anisotropy was optimized within the range found for Mn catalase(III,IV) and other $Mn_2(\mu\text{-}O)_2$ model complexes ($\leq$1% g_e).

Simulations

3Mn(III)−1Mn(IV). (1) The Native MLS. The three basis states, $|^7/_2,4,^1/_2\rangle$ in class I of the dimer-of-dimers model, $|(4)2,^1/_2\rangle$ in class II and $|(4)^5/_2,^1/_2\rangle$ in class III of the distorted-trigonal model are identical (see Table A3 and Supporting Information for proof), and consequently all three give rise to the same set of projections and hence identical spectra. Using this set of projections and the catalase-like hyperfine tensors given in Table 1, we obtained a simulated MLS that is a very poor match to the experimental spectrum; compare Figure 2c to Figure 2a,

(54) Banci, L.; Bertini, I.; Briganti, F.; Luchinat, C.; Scozzafava, A.; Oliver, M. V. *Inorg. Chem.* **1991**, *30*, 4517−4524.
(55) Wemple, M. W.; Tsai, H. L.; Folting, K.; Hendrickson, D. N.; Christou, G. *Inorg. Chem.* **1993**, *32*, 2025−2031.
(56) Cooper, S. R.; Dismukes, G. C.; Klein, M. P.; Calvin, M. *J. Am. Chem. Soc.* **1978**, *100*, 7248−7252.

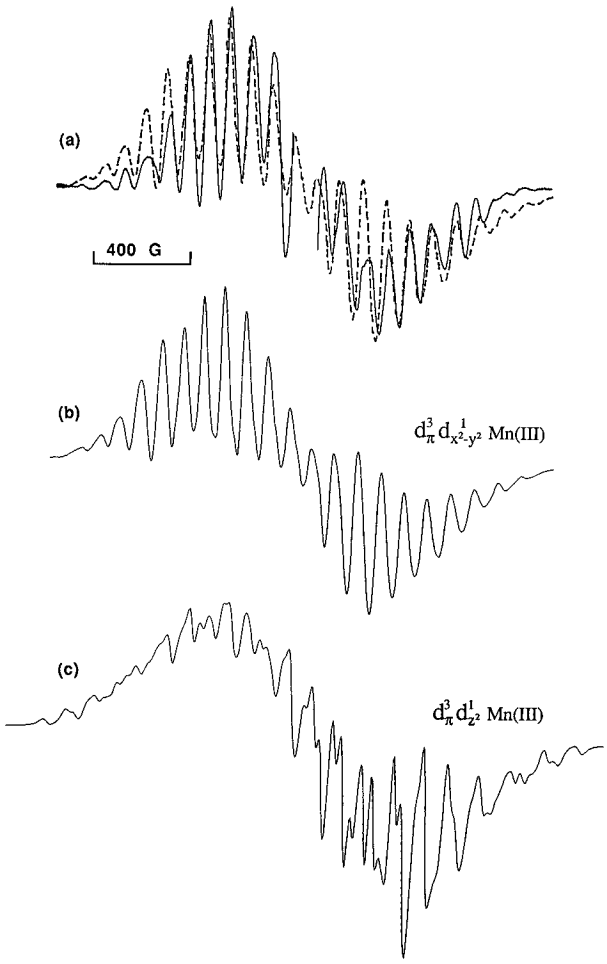

Figure 2. EPR simulations of the native MLS from the 3Mn(III)−1Mn(IV) model. (a) Experimental spectrum (solid line) with simulation b overlaid (dashed line). (b and c) Simulation obtained using catalase-like hyperfine tensors with (b) reversed sign of hyperfine anisotropy corresponding to the $(d_\pi)^3(d_{x^2-y^2})^1$ configuration and (c) the same sign corresponding to the $(d_\pi)^3(d_{z^2})^1$ configuration. See Table 2 for parameters.

respectively. There was no improvement by allowing all four tensors to change by ±5%. However, by reversing the sign of the Mn(III) hyperfine anisotropy for all three tensors and allowing for optimization of the tensor magnitudes by ±5%, the simulated MLS looks remarkably similar to the native MLS in terms of average hyperfine splitting, the number of lines and the intensity pattern, as shown in Figure 2b (and the dashed trace in Figure 2a). The sign change produces a 200% change in the anisotropic part of the hyperfine tensor. Detailed simulation parameters are summarized in Table 2. We found that it is essential to adopt the reversed sign for the hyperfine anisotropy with $A_{||} < A_\perp$ for all three Mn(III) ions in order to obtain the best simulations. If we allow some of the Mn(III) hyperfine tensors to adopt the same anisotropy sign as found in Mn catalase(III,IV), then the simulations become progressively worse approaching that given in Figure 2c where all three Mn(III) tensors have the catalase sign. In our best simulation, all of the hyperfine tensors are collinear with each other. Simulations have also been made in which the unique axis of one or two hyperfine tensors was chosen to be perpendicular to that of the others, but they all give significantly poorer agreement with the experimental spectrum.

(2) NH_3-Bound MLS. The state $|^7/_2,3,^1/_2\rangle$ in class I of the dimer-of-dimers model (Table A3 in Supporting Information) is the only state capable of giving a good simulation of the NH_3-bound MLS when the intrinsic hyperfine tensors are restricted to be nearly equal to the same values used for the native MLS; compare Figure 3a to Figure 3b. All six remaining doublet states produce spectra that are either much too narrow in their total spectral breadth, or have hyperfine patterns very different from the experimental MLS. We also find here again that the intrinsic hyperfine tensors for all three Mn(III) ions must have the opposite sign for the anisotropic part compared to Mn(III) in Mn catalase(III,IV). We found no agreement with the experimental MLS if the sign of the Mn(III) hyperfine anisotropy is assumed to be the same as found in Mn catalase(III,IV); compare Figure 3a to Figure 3c.

(3) Ca^{2+}-Depleted MLS. Simulation of this MLS is problematic. We found that if we continue to use collinear anisotropic hyperfine tensors, no spin state could be found which gives a good simulation. If instead we use isotropic hyperfine couplings, the state $|(^7/_2)^3/_2,^1/_2\rangle$ in class IV of the distorted trigonal model (Table A3) yields a spectrum that only qualitatively resembles both the overall hyperfine breadth and average hyperfine splitting exhibited by the experimental spectrum; compare Figure 4b to Figure 4a. Because Mn EXAFS data have established that there are major structural changes in the Mn_4 cluster upon removal of Ca^{2+} this argues against using the hyperfine and **g** tensor parameters that are restricted to values found in Mn Catalase and the native WOC. Presumably, both the principal values of the tensors and their mutual orientations could have changed. We believe this is the case and that it accounts for the inability of the catalase parameters to give a good simulation of the Ca^{2+}-depleted MLS. The main conclusion we reach is that formation of the Ca^{2+}-depleted MLS also requires a change in the ground spin state to a state with smaller projections from the individual ions, much like what occurs upon NH_3 binding.

3Mn(IV)−1Mn(III). Generally speaking, this oxidation state model gives fewer possible spin states that can fulfill the spectral breadth requirement imposed by eq 8, due to the smaller projections. Of the 28 doublet spin states possible in the four classes that are defined for the dimer-of-dimers and distorted-trigonal models (listed in Table A4), only two have total projections $\sum|p_i| = 5$ and thus can yield an overall hyperfine field in agreement with the experimental breadth. All others doublet states have $\sum|p_i| < 5$ and thus may be dismissed. This constraint is met using the catalase hyperfine tensors including dipolar anisotropy. Use of larger intrinsic hyperfine constants would enable more doublet spin states to be considered; however, the upper limits to the isotropic and dipolar hyperfine constants seen in all Mn(III) complexes examined to date are 227 MHz (81 G) and 65 MHz (23 G), respectively.[15] Even using the largest known intrinsic hyperfine tensors still limits the allowed doublet spin states to only those two having spin projections $\sum|p_i| = 5$. These are the doublet state $|^7/_2,3,^1/_2\rangle$ in the dimer-of-dimers model and $|(^7/_2)2,^1/_2\rangle$ in the distorted-trigonal model (Table A4 in Supporting Information).

(1) The Native MLS. These two basis states in the 3Mn(IV)−1Mn(III) oxidation model are actually identical states and therefore give identical spectra. This state generates a native MLS similar to the experimental spectrum; compare Figure 5b to Figure 5a. The deviation of the intrinsic scalar hyperfine constants from the values for Mn catalase(III,IV) has to be larger than 5% in order to obtain a good simulation. We found that values differing by 10% produce the best agreement, as noted in Figure 5b and Table 3. Once again, the Mn(III) hyperfine anisotropy has to be opposite in sign to that observed in tetragonal ligand fields, *i.e.*, opposite to Mn catalase; compare Figure 5b to Figure 5c.

Table 2. Simulation Parameters for the S_2 Multiline EPR Spectra[a]

		Mn(III)	Mn(III)	Mn(III)	Mn(IV)
native MLS	projection	$P_1 = {}^5/_3$	$P_2 = {}^5/_3$	$P_3 = -{}^4/_3$	$P_4 = -1$
	A_x, A_z	−277, −363	−277, −363	226, 288	250, 226
	a_x, a_z	−166, −218	−166, −218	−170, −216	−250, −226
NH_3-bound MLS	projection	$P_1 = -1$	$P_2 = -1$	$P_3 = {}^{12}/_7$	$P_4 = {}^9/_7$
	A_x, A_z	173, 227	173, 227	−295, −385	−322, −294
	a_x, a_z	−173, −227	−173, −227	−172, −225	−250, −229
Ca^{2+}-depleted MLS	projection	$P_1 = -36/35$	$P_2 = {}^4/_5$	$P_3 = 2$	$P_4 = -{}^{27}/_{35}$
	A_x, A_z	197, 197	−154, −154	−384, −384	183, 183
	a_x, a_z	−192, −192	−192, −192	−192, −192	−237, −237

[a] Oxidation model: 3Mn(III)−1Mn(IV). Native MLS: $|{}^7/_2,4,{}^1/_2\rangle$, $(g_x, g_y, g_z) = (2.01, 2.01, 1.97)$. NH_3-bound MLS: $|{}^7/_2,3,{}^1/_2\rangle$, $(g_x, g_y, g_z) = (1.97, 1.97, 2.01)$. Ca^{2+}-depleted MLS: $|({}^7/_2)^3/_2,{}^1/_2\rangle$, $(g_x, g_y, g_z) = (2.00, 2.00, 2.00)$. Units for hyperfine constants: MHz. (A_x, A_z), (a_x, a_z) are the effective and intrinsic mononuclear hyperfine tensors, respectively.

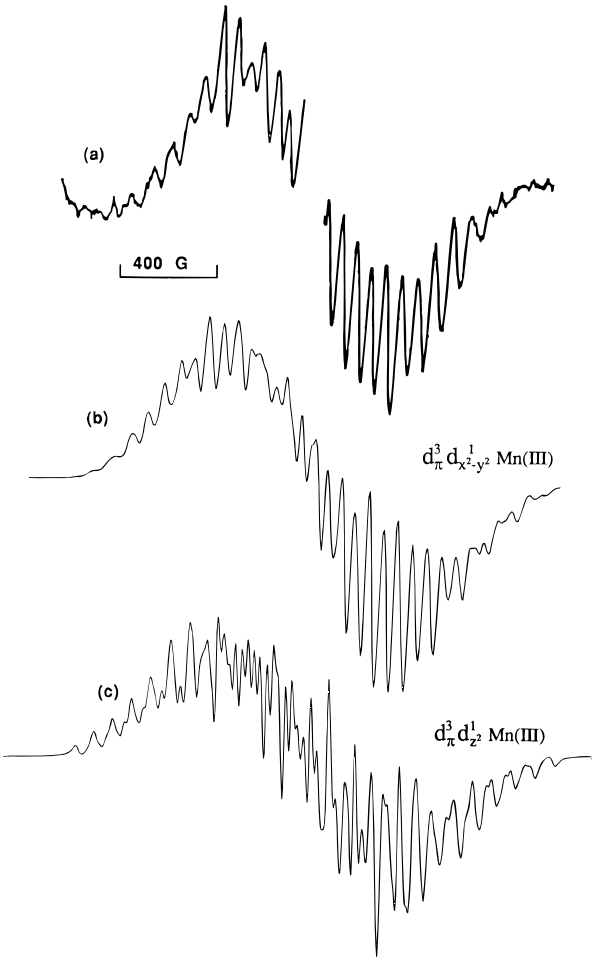

Figure 3. Simulations of the NH_3-bound MLS for the 3Mn(III)−1Mn(IV) model. (a) Experimental spectrum. (b and c) Simulation obtained using catalase-like hyperfine tensors with (b) reversed sign of hyperfine anisotropy corresponding to the $(d_\pi)^3(d_{x^2-y^2})^1$ configuration and (c) the same sign corresponding to the $(d_\pi)^3(d_{z^2})^1$ configuration. See Table 2 for parameters.

(2) NH_3-Bound MLS. No spin state could be found which gives a reasonable simulation of this form of MLS using the same Mn(III) and Mn(IV) hyperfine tensors of Mn catalase-(III,IV), and with either sign for the anisotropy. The simulated spectra have either different hyperfine patterns or narrower total spectral width as compared to the experimental spectrum. We examined a range of intrinsic hyperfine tensors differing by as much as ±15% from the Mn catalase(III,IV) values and both positive and negative signs for the Mn(III) anisotropy.

(3) Ca^{2+}-Depleted MLS. The basis state $|(3)^3/_2,{}^1/_2\rangle$ in the distorted-trigonal model (Table A4) gives an approximate simulation of this MLS. Here again we found that using anisotropic hyperfine tensors analogous to Mn catalase (±10%) we were unable to get good simulations, reflecting, we believe, the expected change in principal values or orientations of the tensors or both. However, using isotropic hyperfine constants again we see that a qualitative simulation may be obtained; compare Figure 4c to Figure 4a. The main feature which can be reproduced is the 25% contraction in the mean hyperfine splitting, a feature which is due to the reduced projections in this lower spin state.

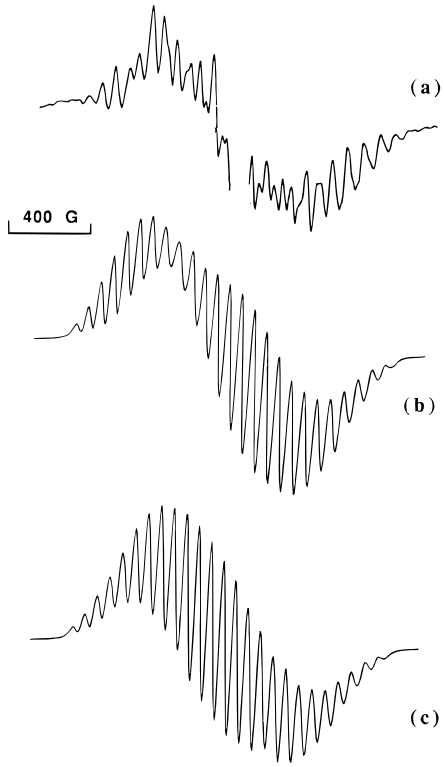

Figure 4. Simulations of the Ca^{2+} depleted MLS. (a) Experimental spectrum. (b) Simulation obtained for the 3Mn(III)−1Mn(IV) model using isotropic hyperfine parameters. See Table 2 for parameters. (c) Simulation obtained for the 3Mn(IV)−1Mn(III) model. See Table 3 for parameters.

Q-Band and S-Band EPR Spectra of the Native MLS. Using the same approach we generated simulated spectra at Q-band frequencies (34 GHz), which agrees well with the experimental spectrum (data not shown).

In the case of the S-band spectrum, experiment reveals a large number (40−50) of resolved splittings which have anisotropic line shapes and have been attributed to ^{55}Mn hyperfine anisotropy.[57] At 3 GHz the Zeeman interaction is smaller than the

(57) Haddy, A.; Aasa, R.; Andreasson, L.-E. *Biochemistry* **1989**, *28*, 6954−6959.

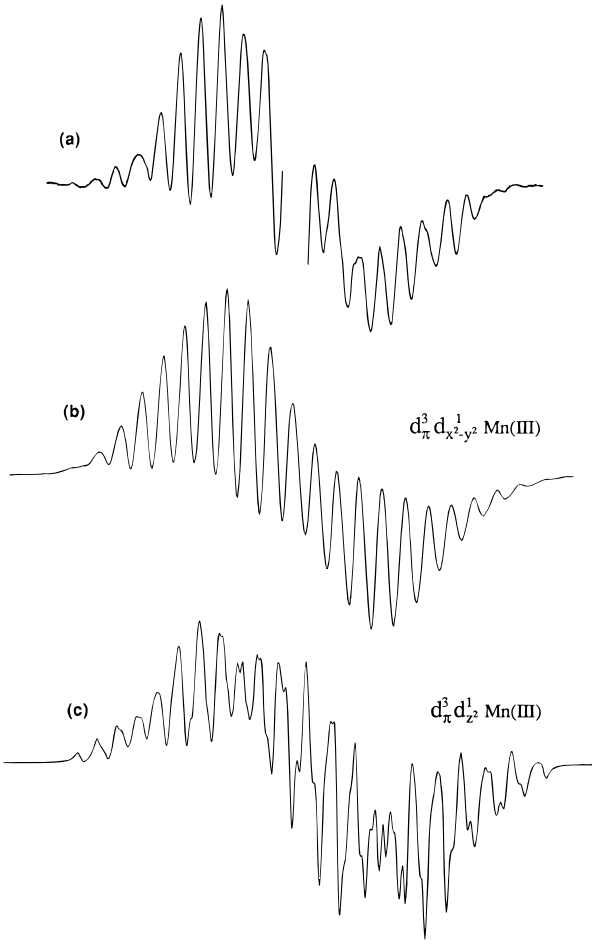

Figure 5. Simulations of the native MLS for the 3Mn(IV)−1Mn(III) model. (a) Experimental spectrum. (b and c) Simulation obtained using catalase-like hyperfine tensors with (b) reversed sign of hyperfine anisotropy corresponding to the $(d_\pi)^3(d_{x^2-y^2})^1$ configuration and (c) the same sign corresponding to the $(d_\pi)^3(d_{z^2})^1$ configuration. See Table 3 for parameters.

total hyperfine field. Hence, the simulation method we use is not accurate at such a low frequency owing to the limitation to second order corrections in $A^2/(g\beta H)$.

Discussion

Oxidation States of the Mn Ions. The simulations presented in this work better support the 3Mn(III)−1Mn(IV) (lower) oxidation state model for the S_2 state. Compared to the 3Mn(IV)−1Mn(III) oxidation state model the lower oxidation model allows for larger hyperfine fields owing to the larger spin projections. For example, in the dimer-of-dimers model (class I in Table A3 and A4) we have projections $-4/3$, -1, $5/3$, and $5/3$ for state $|7/2,4,1/2\rangle$ in a 3Mn(III)−1Mn(IV) model vs $12/7$, $9/7$, -1, and -1 for state $|7/2,3,1/2\rangle$ in the higher oxidation model, corresponding to a 12% smaller hyperfine field. This difference is the same reason why there is a 25% increase in the hyperfine field observed in going from $Mn^{III}Mn^{IV}$ to $Mn^{II}Mn^{III}$ binuclear sites.[11,15]

The general argument given above is supported by the EPR simulations. The 3Mn(III)−1Mn(IV) model gives good simulations for both major types of MLS using a set of hyperfine tensors whose scalar traces are close to those found for Mn(III) and Mn(IV) ions having closely similar ligand types (the anisotropic part is discussed in the next section). By contrast, the 3Mn(IV)−1Mn(III) model requires larger scalar hyperfine couplings (>10% larger) to allow simulation of the native MLS and could not provide any spin state capable of accounting for the NH_3-bound MLS. These hyperfine couplings are larger than those found for the model compounds having similar ligand types.

Mn oxidation state assignments for the S states have also been proposed on the basis of flash-induced visible absorption changes, water proton T_1 relaxivity data and Mn XANES spectroscopy (summarized in ref 1). The first two methods do not provide an unambiguous answer and will not be discussed further. The results from Mn XANES have been interpreted to favor either 4Mn(III)[58] or 2Mn(III)−2Mn(IV) for the S_1 state,[59,60] while direct measurements on the S_2 state have favored 3Mn(IV)−1Mn(III).[59] These results require interpretation of the 1s-electron ionization energies based on comparison with model complexes for which there is considerable overlap between Mn(III) and Mn(IV) complexes of varying ligand fields. As a result, the odd-spin nature of the S_2 oxidation state deduced from EPR analysis of the MLS has factored into the interpretation of the XAS edges.

Moreover, it appears that none of the published data sets considered thus far has included five-coordinate Mn ions. All data are on six-coordinate complexes of Mn(III) and Mn(IV). As we shall discuss below, the Mn(III) hyperfine anisotropy data suggest the presence of five-coordinate Mn(III) ions. The reduction in coordination number from six to five leads to an increase in the ionization potentials of the Mn electrons. We expect that the shift to higher binding energy would be sufficient (1 eV would be enough) to cause the Mn(III) K edge to fall in the range of six-coordinate Mn(IV) ions. Because only six-coordinate compounds have been used to obtain a correlation between K edge energies and formal oxidation states, this correlation will lead to an incorrect (higher) oxidation state to be assigned to five-coordinate Mn ions.

Electronic Configuration of Mn(III) and Its Implications. In both oxidation state assignments for the S_2 state, we found that for simulations of both the native MLS and the NH_3-bound MLS (lower oxidation state only) the sign of the anisotropic part of the Mn(III) hyperfine tensor must be reversed from that observed for conventional tetragonally elongated six-coordinate Mn(III) ions, such as found in Mn catalase(III,IV). For Mn(III) in a tetragonal ligand field, this sign reversal corresponds, according to ligand field theory, eq 2, to a switch in electronic configuration from $(d_\pi)^3(d_{z^2})^1$ to $(d_\pi)^3(d_{x^2-y^2})^1$. Schematic representations of the proposed spatial arrangements for the valence $(d_\pi)^3(d_{z^2})^1$ and $(d_\pi)^3(d_{x^2-y^2})^1$ orbitals relative to the ligand fields in six-coordinate $(\mu\text{-O})_2$ bridged Mn dimers are given in Chart 2. The usual $(d_\pi)^3(d_{z^2})^1$ configuration found in six-coordinate complexes leads to strong bonding in the plane orthogonal to the d_{z^2} orbital. Strong bonding within the $[Mn_2O_2]^{3+/4+}$ cores of many complexes has been widely observed and is believed to be responsible for the planarity of the Mn_2O_2 rhombus, the kinetic stability to ligand substitution, and the low oxidative reactivity exhibited by most μ-oxo bridges in transition metal clusters.[61]

A strong tetragonal compression along the Mn-ligand axis orthogonal to the $[Mn_2O_2]^{3+/4+}$ rhombus, coupled with an in-plane expansion of the core would lower the energy of the $d_{x^2-y^2}$ orbital and raise the d_{z^2} orbital, resulting in occupation of $d_{x^2-y^2}$.

(58) Kusunoki, M.; Ono, T.-A.; Matsushita, T.; Oyanagi, H.; Inoue, Y. *J. Biochem.* **1990**, *108*, 560−567.
(59) Yachandra, V. K.; DeRose, V. J.; Latimer, M. J.; Mukerjee, I.; Sauer, K.; Klein, M. P. *Photochem. Photobiol.* **1991**, *53*, 98−99.
(60) Riggs, P. J.; Mei, R.; Yocum, C. F.; Penner-Hahn, J. E. *J. Am. Chem. Soc.* **1992**, *114*, 10650−10651.
(61) Nugent, W. A.; Mayer, J. M. *Metal-ligand multiple bonds: the chemistry of transition metal complexes containing oxo, nitrido, imido, alkylidene or alkylidyne ligands*; John Wiley: New York, 1988; p 324.

Table 3. Simulation Parameters for the S_2 Multiline EPR Spectra[a]

		Mn(IV)	Mn(IV)	Mn(III)	Mn(IV)
native MLS	projection	$P_1 = -1$	$P_2 = -1$	$P_3 = {}^{12}/_{7}$	$P_4 = {}^{9}/_{7}$
	A_x, A_z	237, 237	237, 237	−257, −337	−280, −300
	a_x, a_z	−237, −237	−237, −237	−150, −197	−218, −233
Ca^{2+}-depleted MLS	projection	$P_1 = -{}^{4}/_{5}$	$P_2 = -{}^{4}/_{5}$	$P_3 = 2$	$P_4 = {}^{3}/_{5}$
	A_x, A_z	190, 190	190, 190	−384, −384	−142, −142
	a_x, a_z	−237, −237	−237, −237	−192, −192	−237, −237

[a] Oxidation model: 3Mn(IV)−1Mn(III). Native MLS: $|{}^{7}/_{2},3,{}^{1}/_{2}\rangle$, $(g_x, g_y, g_z) = (2.00, 2.00, 1.98)$. Ca^{2+}-depleted MLS: $|(3){}^{3}/_{2},{}^{1}/_{2}\rangle$, $(g_x, g_y, g_z) = (2.00, 2.00, 2.00)$. Units for hyperfine constants: MHz. (A_x, A_z), (a_x, a_z) are the effective and intrinsic mononuclear hyperfine tensors, respectively.

Chart 2

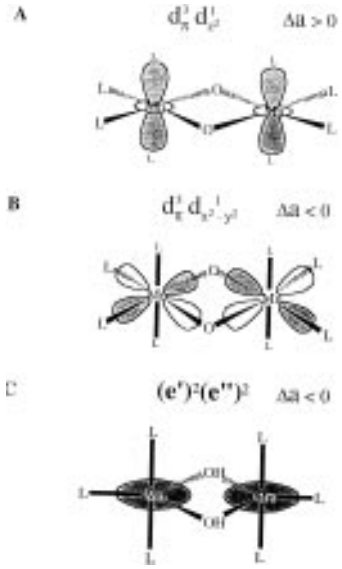

In this new configuration the Mn−(μ-O)$_2$−Mn bonds would be weakened and thus could offer a possible means for activating the oxo bridges for oxidative coupling by lowering the barrier to dioxygen release. However, the $(d_\pi)^3(d_{x^2-y^2})^1$ configuration has never been reported to our knowledge for any six-coordinate Mn(III) complex (reverse Jahn−Teller distortion), with the possible exception of manganese tris(acetylacetonate) ([CH_3-COCH=C(O−)CH_3]$_3$Mn), for which structural data indicate a tetragonal compression.[62] Unfortunately, we are unaware of data on the electronic configuration of this complex. The difference in energy between the tetragonally extended $(d_\pi)^3$-$(d_{z^2})^1$ ground state configuration in MnF_6^{3-} and the (unobserved) tetragonally compressed configuration can be estimated to be twice the Jahn−Teller energy or *ca.* 7000 to 8000 cm^{-1}.[63] Of course, the lack of examples for structurally characterized (*i.e.*, stable) tetragonally compressed Mn(III) ions does not provide much support against their possible presence in the WOC where a highly reactive Mn_4 cluster exists.

Reversal in sign of the hyperfine anisotropy from that found in tetragonally extended Mn(III) ions is a natural outcome in five-coordinate ligand fields having trigonal bipyramidal geometry. In D_{3h} site symmetry the 3d valence orbitals split into three sets, a′(d_{z^2}) and two pairs of doubly degenerate orbitals e′($d_{x^2-y^2}$, d_{xy}) and e″(d_{xz}, d_{yz}). In the simplest case with all five ligands equivalent, a′(d_{z^2}) is the lowest unoccupied orbital (LUMO) for a Mn(III) ion (Chart 3). The valence electronic configuration is then $e'^2e''^2$, which is essentially identical to the $(d_\pi)^3(d_{x^2-y^2})^1$ configuration in tetragonal symmetry as far as the electron spin density distribution is concerned. Therefore, in this case the sign of the Mn(III) hyperfine anisotropy would also be opposite to that for the $(d_\pi)^3(d_{z^2})^1$ configuration seen in Mn catalase and all other six-coordinate Mn(III) complexes were structural/electronic data are available. As depicted in Chart 3, the elevation of the a′(d_{z^2}) orbital above the energy of the e′ set is a natural consequence of having one fewer ligand in the equatorial plane and does not require an unusually strong axial ligand field compared to the tetragonally compressed six-coordinate case. Hence, the ligand field potential around the Mn(III) may not be abnormal at all, provided that it is trigonal bipyramidal. We cannot distinguish between these two possible ligand fields on the basis of the ^{55}Mn hyperfine anisotropy alone. However, we can confidently conclude that the conventional $(d_\pi)^3(d_{z^2})^1$ configuration appears not to be present.

Chart 3

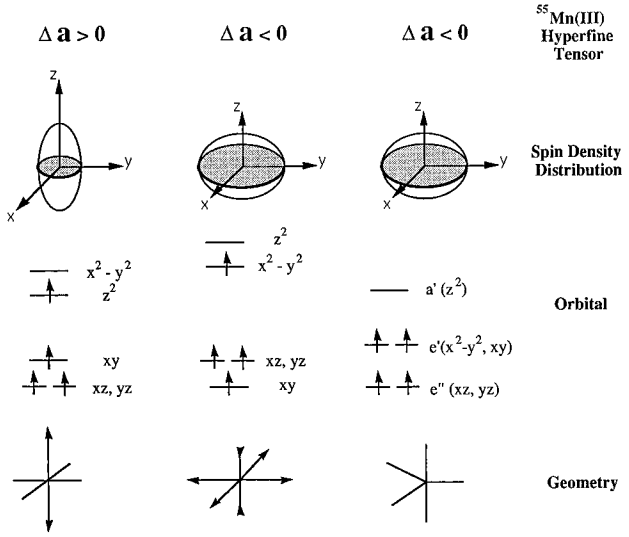

The orbital energies for five-coordinate Mn(III) ions shown in Chart 3 are not from calculations and are not to scale. They are obtained under the assumption that the ligand-field strengths of all ligands are approximately equal. It is therefore unlikely to be true for bis(μ-oxo)-bridged Mn dimers, in which oxos are stronger ligands than others. A bis(μ-hydroxo) core would be more appropriate (see also Chart 1c). As we will discuss later, such a core structure is also favored by our magnetic coupling model.

Five-coordinate Mn(III) ions, although rare in biology, have been observed in one structurally characterized case—Mn superoxide dismutase.[64] In SOD, Mn(III) in its native state is coordinated to protein ligands from three N donors and one O donor and to one H_2O (or OH^-) in a distorted-trigonal bipyramidal geometry. A magnetic circular dichroism study has revealed that Mn(III) has the $(d_\pi)^3(d_{x^2-y^2})^1$ (*i.e.*, $e'^2e''^2$ in

(62) Fackler, J. J. P.; Avdeef, A. *Inorg. Chem.* **1974**, *13*, 1864−1875.
(63) Englman, R. In *The Jahn-Teller Effect in Molecules and Crystalls*; Wiley-Interscience: London, 1972; p 322.
(64) Stallings, W. C.; Pattridge, K. A.; Strong, R. K.; Ludwig, M. L. *J. Biol. Chem.* **1985**, *260*, 16424−16432.

trigonal bipyramid site symmetry) electronic configuration in its native five-coordinate state.[65]

One possible explanation for why there could be five-coordinate Mn(III) ions in the S_2 state of the WOC is that one or both of the substrate water molecules may not be bound yet to the Mn_4 cluster. Restricting the coordination number to less than six is one way to achieve a higher oxidation potential, and this might be needed to achieve the oxidation of water.

Consequences of NH_3 Binding and Ca^{2+} Depletion. As was pointed out in the **Simulations** section the dimer-of-dimers exchange coupling model provides two spin states capable of simulating both the native MLS and the NH_3-bound MLS only for the 3Mn(III)−1Mn(IV) oxidation state. Since the binding of ammonia can occur at a temperature as low as 198 K[66] and is reversible,[67] it is unlikely to induce a major structural change in the Mn_4 cluster. Consequently, we expect that a single exchange coupling model should be adequate to describe both the native and NH_3-bound Mn_4 cluster, as we find for the dimer-of-dimers coupling model. According to the spin state probability diagram in Figure 2, ammonia binding would have to increase the antiferromagnetic character of J_{34} (shift to the left side of the abscissa) in order that the doublet state $|^7/_2,3,^1/_2\rangle$ becomes the new ground state. This indicates that one of the Mn pairs involving the unique Mn(IV) site is more strongly perturbed than the other two.

We interpret formation of the Ca^{2+}-depleted MLS as follows. Calcium depletion from the native enzyme induces a major change in the structure of the Mn_4 cluster which shows up clearly in EXAFS experiments.[3] This structure change leads to a loss of the dimer-of-dimers symmetry and requires also a change of the magnetic model to the distorted-trigonal exchange coupling model or possibly one of even lower symmetry. More importantly, deformation of the native structure presumably results in changes to the ligands or twisting of the Mn hyperfine tensor axes so that there is greater heterogeneity to the hyperfine tensors which we cannot predict by the constrained simulation method we have adopted. This deformation produces a smearing of the anisotropy, with the result that adopting isotropic hyperfine constants for all four Mn ions can give an approximate simulation. The observed 25% decrease in hyperfine splitting still requires a spin state change to a doublet state of lower component spins, regardless of the model one uses.

Dimer-of-Dimers Coupling Model and Correspondence to the Structural Models. We have shown that the spin state $|^7/_2,4,^1/_2\rangle$, with the largest intradimer spin quantum numbers, is capable of generating the native MLS. We have also shown in the spin phase diagram of Figure 1 that in order to have this spin state as the ground state, one has to have at least $J_{34} > 0$, *i.e.*, ferromagnetic. In our oxidation state model S_{34} corresponds to the spin from a pair of Mn(III) ions. Magnetic susceptibility data on $[Mn_2(\mu\text{-}O)_2]^{2+}$ cores in the literature is rare, although there is an abundance of data on $[Mn_2(\mu\text{-}O)_2]^{3+/4+}$ cores which all exhibit strong antiferromagnetic coupling ($2J \sim -200$ to -300 cm^{-1}).[68−70] However, in a recent work the $[Mn_2(\mu\text{-}O)_2]^{2+}$ core was also found to have strong antiferromagnetic coupling ($2J \sim -200$ cm^{-1}).[71] Thus there is an *apparent* discrepancy between the predicted ferromagnetic J_{34} (positive sign) of the Mn_4 tetramer model and the observed antiferromagnetic coupling (negative sign) seen in one example of the simple dimeric $[Mn_2(\mu\text{-}O)_2]^{2+}$ core.

What is the relationship between the sign of the exchange interaction in a dimer vs a tetramer? To answer this question, one must examine under what conditions the general six-J exchange Hamiltonian of eq 4 can be contracted into, *i.e.*, approximated by, the three-J dimer-of-dimers Hamiltonian of eq 5. Belinski has given the matrix elements of the true exchange Hamiltonian (eq 4) in the dimer-of-dimers basis representation $|S_{12},S_{34},S_T\rangle$ (eq 23 to eq 28 of ref 41). It can be shown from these matrix elements that if, and only if, j_{13}, j_{23}, j_{14}, and j_{24} are about the same magnitude, the general six-J exchange Hamiltonian of eq 4 can be approximated by the three-J dimer-of-dimers Hamiltonian of eq 5 with the correspondence given by

$$J = {}^1/_4(j_{13} + j_{23} + j_{14} + j_{24})$$

$$J_{12} = j_{12} - {}^1/_4(j_{13} + j_{23} + j_{14} + j_{24}) \qquad (9)$$

$$J_{34} = j_{34} - {}^1/_4(j_{13} + j_{23} + j_{14} + j_{24})$$

These equations give the effective dimer-of-dimers exchange coupling constants (J_{ij}) in terms of the real pair-wise exchange coupling constants (j_{ij}). According to eq 9, there are two ways of getting an effective ferromagnetic coupling $J_{34} > 0$ as required by the simulations: (1) if $j_{34} > 0$, and $(j_{13} + j_{23} + j_{14} + j_{24}) < 0$ or its absolute value is small compared to j_{34}; (2) if $j_{34} < 0$ and ${}^1/_4(j_{13} + j_{23} + j_{14} + j_{24}) > |j_{34}| > 0$. Are these coupling cases compatible with the dimer-of-dimers structural model derived from EXAFS, in which two strongly coupled $Mn_2(\mu\text{-}O)_2$ cores interact weakly at a single bridging position? The first method requires ferromagnetic intradimer coupling within at least one of the $[Mn_2(\mu\text{-}O)_2]^{2+,3+,4+}$ cores. But ferromagnetic couplings are incompatible with magnetically isolated $Mn_2(\mu\text{-}O)_2$ cores, which are known to be strong antiferromagnets. The second method retains intradimer antiferromagnetic coupling, but requires strong interdimer coupling, which is again hard to realize in the simplest structural model.

It may be possible to reconcile the magnetic and structural models. The dimer-of-dimers model could be structurally correct in terms of intermanganese distances and number of Mn scattering partners but magnetically incorrect in terms of assuming six-coordinate $Mn_2(\mu\text{-}O)_2$ cores with antiferromagnetic intradimer couplings. Ferromagnetic intradimer couplings would be more favored if only one μ-oxo bridge exists or if the proposed μ-oxo's are protonated, *i.e.*, μ-hydroxo's. μ-oxo's are not distinguishable from μ-hydroxo's or any other second row atom by the available EXAFS data. Indeed a study has shown that protonation of six-coordinate $Mn_2(\mu\text{-}O)_2$ cores results in a dramatic decrease in antiferromagentic coupling, but at the same time gives rise to an increase of 0.2 Å in Mn−Mn separation.[72] Such a large increase would be readily detected by EXAFS. Only if the protein environment were to constrain the Mn−Mn separation to 2.7 Å would it be possible to propose a bis(μ-hydroxo) bridge between six-coordinate Mn ions in explanation of the ferromagnetic coupling. The hyperfine anisotropy data point to either five-coordinated Mn(III) ions or

(65) Whitaker, J. W.; Whitaker, M. M. *J. Am. Chem. Soc.* **1991**, *113*, 5528−5540.
(66) Boussac, A.; Rutherford, A. W.; Styring, S. *Biochemistry* **1990**, *29*, 24−32.
(67) Beck, W. F.; Brudvig, G. W. *Biochemistry* **1986**, *25*, 6479−6486.
(68) Christou, G. *Acc. Chem. Res.* **1989**, *22*, 328−335.
(69) Wieghardt, K. *Angew. Chem., Int. Ed. Engl.* **1989**, *28*, 1153−1172.
(70) Hagen, K. S.; Westmoreland, T. D.; Scott, M. J.; Armstrong, W. H. *J. Am. Chem. Soc.* **1989**, *111*, 1907−1908.
(71) Glerup, J.; Gooson, P. A.; Hazell, A.; Hazell, R.; Hodgson, D. J.; McKenzie, C. J.; Michelsen, K.; Rychlewska, U.; Toftlund, H. *Inorg. Chem.* **1994**, *33*, 4105−4111.
(72) Baldwin, M. J.; Stemmler, T. L.; Riggs-Gelasco, P. J.; Kirk, M. L.; Penner-Hahn, J. E.; Pecoraro, V. L. *J. Am. Chem. Soc.* **1994**, *116*, 11349−11356.

Chart 4

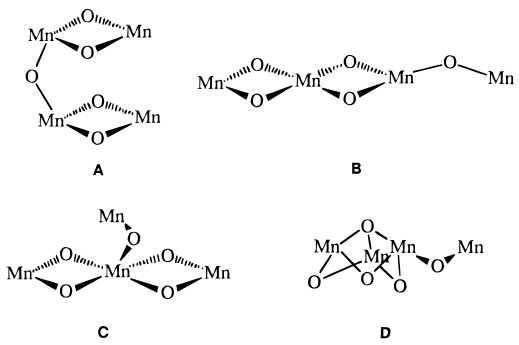

strained six-coordinate Mn(III) ions. Hence, a logical solution would be a five-coordinate $Mn_2(\mu\text{-}OH)_2$ core, such as depicted in Chart 2c.

Alternatively, one of the less-favored structural models proposed on the basis of the EXAFS data that is also consistent with the magnetic data needs to be considered. The four structural models that have been proposed on the basis of EXAFS data are depicted in Chart 4.[52] Of these models we can rule out A and B, since both predict magnetic ground states that have too small hyperfine projections to account for the MLS. Structural models **C** and **D** lead to different magnetic models than the two we have considered in this work (Chart 1). Thus, we do not know if either is capable of predicting the unusually large hyperfine fields needed to explain the major forms of the MLS.

Before ending this part of the discussion let's examine a related exchange coupling problem found in the 4Fe−4S proteins. 4Fe−4S clusters usually have cubane structures, so it's not obvious at all that a dimer-of-dimers coupling scheme could be used to describe the exchange couplings. However, Middleton et al. have shown that a dimer-of-dimers coupling scheme explains quite well the EPR and Mossbauer spectra from the reduced ferredoxin (3Fe(II)−1Fe(III) center) from *Bacillus stearothermophilus*.[73] With this in mind, we again emphasize that a dimer-of-dimers exchange model does not necessarily exclude structural models other than dimer-of-dimers type.

The State Responsible for the Native MLS Is a Pure Eigenstate, even for Lower Symmetry Cases. The spin state $|^7/_2,4,^1/_2\rangle$ from the dimer-of-dimers coupling scheme in the 3Mn(III)−1Mn(IV) oxidation model provides a remarkably good simulation of the native MLS, owing to its large spin projections from each ion. But what about eignestates from lower symmery exchange models? Would they also provide good simulations? There is an important feature of this particular state which makes it an eigenstate even in lower cluster symmetries and thus independent of the choice of the coupling model. First, this state occupies the largest area in the spin phase diagram (Figure 2) among all the spin eigenstates, indicating that it is the most probable ground state in the dimer-of-dimers coupling scheme if the intradimer couplings, J_{12} and J_{34}, are randomly chosen. Second, lowering the symmetry of the exchange Hamiltonian from the dimer-of-dimers coupling scheme produces no mixing of $|^7/_2,4,^1/_2\rangle$ with any of the other doublet spin states, if in the general exchange Hamiltonian eq 4 the condition $j_{13} \sim j_{23}$ and $j_{14} \sim j_{24}$ is maintained. This has been proven by Belinskii.[41] Accordingly, the dimer-of-dimers model will predict the correct magnetic properties (EPR spectrum, etc.) for this eigenstate even if the exchange Hamiltonian has rhombic symmetry.

Comparison with Other MLS Simulations. Our EPR simulations of dimanganese model complexes and catalase[15] do not support the large value chosen by Kusunoki for the Mn(III) hyperfine constant (94.5 G) or the assumption of scalar coupling.[16] First, we found that all Mn(III) ions possess substantial hyperfine anisotropy, typically 30% of the isotropic value.[15] Second, the isotropic part of the Mn(III) hyperfine interaction is well below 90 G for all complexes; for Mn(III) in Mn catalase(III,IV) this is 68.5 G, about 40% less than Kusunoki's choice for the WOC. The reason why Kusunoki's choice for the isotropic hyperfine parameters is so large is due in part to his implicit assumption that the Mn ions in the $[Mn_2(\mu\text{-}O)_2]^{2+/3+/4+}$ cores of the Mn_4 cluster are antiferromagnetically coupled. This leads to a choice of very large hyperfine constants because his spin state, a mixture of $|^1/_2,0,^1/_2\rangle$ and $|^1/_2,1,^1/_2\rangle$, has smaller projection numbers. As we have shown in a previous section, antiferromagnetic coupling in the $[Mn_2(\mu\text{-}O)_2]^{2+/3+/4+}$ units can become ferromagnetic coupling within Mn_4 clusters having at least four exchange pathways. Therefore, Kusunoki's assumption is not always true.

The oxidation model, 3Mn(III)−1Mn(IV), which our anisotropic simulations favor for the S_2 state, differs from Kusunoki's choice of 3Mn(IV)−1Mn(III) based on isotropic EPR simulations. Curiously, their oxidation model derived from EPR simulations for the S_2 state differs from their assignment of 3Mn(III)−1Mn(IV) deduced from Mn XANES data from the same laboratory.[58] This discrepancy has not been addressed by the authors.

Like Kusunoki, Bonvoisin et al. also used isotropic g and Mn hyperfine couplings to simulate the native MLS. By using a nonlinear least-squares searching method, they were able to identify two sets of isotropic hyperfine parameters which gave the closest fits to the position of the major peaks of only the native MLS.[14] However, if realistic anisotropic tensors were used, the fitting parameters would definitely be quite different. Since the two sets of effective hyperfine parameters they obtained were not analyzed in terms of an exchange coupling scheme, oxidation level or intrinsic hyperfine constants, no molecular insight was extracted and no further comparison with the present study can be made.

A recent model by Åhrling and Pace has considered the possibility that the much greater hyperfine field (spectral breadth) of the native MLS and its complex superhyperfine structure—the latter has not been addressed in our work—could arise, in principal, from a simple Mn dimer if forbidden EPR transitions were to become allowed through the presence of very large ^{55}Mn nuclear-electric quadrupole interactions and unusually large scalar and anisotropic hyperfine couplings. They included simulations of the native MLS at S-, X-, and Q-band frequencies, but only the X- and Q-band simulations were of good quality. They did not consider if their model could explain the NH_3-bound or Ca^{2+}-depleted forms of the MLS. It is noteworthy that there are no synthetic Mn complexes which come even close to having the required magnetic parameters of this hypothetical species. For example, the isotropic hyperfine constants (a_{iso}) in their model are −229 and −257 MHz for Mn(III) and Mn(IV), respectively, while the hyperfine anisotropies are 104% and 88% of a_{iso}. The latter anisotropies are 3−4× and 9−10× larger, respectively, than found in a series of model complexes or varying O/N ligand ratio.[15] Also, the principal values of the nuclear electric quadrupole interaction tensor which they use are −21 to +49 MHz and −24 to +51 MHz for Mn(III) and Mn(IV), respectively. These values are 20−50 times larger than the measured values obtained for the

(73) Middleton, P.; Dickson, D. P. E.; Johnson, C. E.; Rush, J. D. *Eur. J. Biochem.* **1978**, *88*, 135−141.

(74) Zheng, M.; Dismukes, C. Unpublished results.

native MLS using both high frequency (0−250 MHz) CW-ENDOR spectroscopy ($(3e^2qQ)/(4I(I-1)) \sim 2$ MHz for Mn(IV)[74]) and pulsed-ENDOR spectroscopy ($(3e^2qQ)/(4I(I-1)) \sim 1$ MHz[75]). Moreover, our group and Britt's group have measured two synthetic dimanganese(III,IV) complexes containing the $Mn_2(\mu\text{-}O)_2^{3+}$ core and obtained values between 0.3 and 1 MHz. We conclude that the parameters chosen by Åhrling and Pace to achieve simulation of the native MLS are highly improbable and, in our view, negate the validity of their dimer model.

Conclusions

We have provided a theoretical framework and simulation procedure for interpretation of the various multiline EPR signals from the Mn_4 cluster in PSII. Excellent simulations have been obtained using realistic intrinsic hyperfine tensors for Mn ions. Our results strongly suggest 3Mn(III)−1Mn(IV) as the correct oxidation state assignment for the S_2 state in Kok's scheme of oxygen evolution. More important, we have obtained the first evidence identifying the electronic orbital configuration of the valence electrons associated with the Mn(III) ions. In both the native and NH_3-bound forms of the S_2 state the Mn(III) ions possess an unusual electron spin distribution corresponding to the $(d_\pi)^3(d_{x^2-y^2})^1$ configuration in a six-coordinate environment, or alternatively the $(e')^2(e'')^2$ configuration in a trigonal-bipyramidal geometry. Both cases offer insights which may explain the unique oxidative reactivity of the Mn_4 cluster in the WOC. The magnetic model needed to explain all three MLS is incompatible with the simplest structural model deduced from EXAFS studies in which two isolated $Mn_2(\mu\text{-}O)_2$ dimers interact weakly at a single bridging site.

The significance of these conclusions depend on whether the assumptions of the model are valid. We have made only two basic assumptions: (1) we use realistic intrinsic hyperfine tensors for all Mn ions, in contrast to most prior simulations. The ±15% range of anisotropies we have explored is based on EPR simulations of numerous model compounds and Mn catalase. ^{55}Mn ENDOR measurements have also confirmed the EPR measured hyperfine anisotropy for Mn(III) in two model dimers and the native MLS.[76] (2) We have adopted two simplified Heisenberg exchange coupling schemes for the Mn_4 cluster in PSII. One of these magnetic models, the dimer-of-dimers, is isomorphic to one of the structural models deduced by X-ray absorption studies by Klein et al. and others. We have demonstrated that only two of the resulting basis states can contribute to the electronic ground state which we ascribe to the MLS. We have noted in the text that both exchange models can be generalized to include the mixing of basis states under lower symmetry exchange couplings, and that one of the two basis states is unaffected. Thus, the exchange model has wider applicability than the simple dimer-of-dimers symmetry. Each of these "assumptions" is noted in the text.

Acknowledgment. This research was supported by the National Institutes of Health, Institute of General Medicine, GM-39932. We thank Prof. D. Britt for permission to use a copy of his NH_3-bound MLS spectrum and for sharing preliminary ^{55}Mn ENDOR data, Prof. N. Kitajima for providing a model complex, and Drs. M. Klein, K. Sauer, and M. Kusunoki for preprints.

Supporting Information Available: Text giving (1) vector coupling expressions for p_i projections, (2) correspondence between the dimer-of-dimers and distorted trigonal models and comment on the model of Kusunoki et al., (3) construction of the spin phase diagram, and (4) classification of tetramer spin states. Scheme A3 (vector coupling cases for Mn tetramer) and Table A2 (coupling cases classified), Table A3 (doublet spin eigenstates for the 3Mn(III)−1Mn(IV) case), and Table A4 (doublet spin eigenstates for the 1Mn(III)−3Mn(IV) case) (11 pages). Ordering information is given on any current masthead page.

IC9512340

(75) Randall, D. W.; Sturgeon, B. E.; Ball, J. A.; Lorigan, G. A.; Chan, M. K.; Klein, M. P.; Armstrong, W. H.; Britt, R. D. *J. Am. Chem. Soc.* **1995**, *117*, 11780−11789.

(76) Zheng, M.; Dismukes, C. Unpublished results.